Macromolecules

ARTICLE

pubs.acs.org/Macromolecules

Mechanism of Halogen Exchange in ATRP

Chi-How Peng, Jing Kong, Florian Seeliger, and Krzysztof Matyjaszewski*

Center for Macromolecular Engineering, Department of Chemistry, Carnegie Mellon University, Pittsburgh, Pennsylvania 15213, United States

Supporting Information

ABSTRACT: Detailed mechanistic studies reveal that halogen exchange (HE) in ATRP can occur not only by a radical pathway (atom transfer) but also by an ionic pathway (S_N2 reaction) because $Cu^{(I)}(L)X$ and $Cu^{(II)}(L)X_2$ complexes contain weakly associated halide anion that can participate in the S_N2 reaction with alkyl halide (ATRP initiator). Both pathways were kinetically studied, and their contributions to the HE process were quantitatively evaluated for seven alkyl halides and three $Cu^{(I)}(L)Cl$ complexes. Radical pathway dominates the HE process for 3° and 2° alkyl bromides with more active complexes such as $Cu^{(I)}(TPMA)Cl$. Interestingly, ionic pathway dominates for 1° alkyl bromides and less active ATRP catalysts. These studies also revealed that degree of association of alkyl halide anion depends on the structure of copper complexes. In addition, radical pathway is accompanied by the reverse reactions such as deactivation of radicals to alkyl bromides and also activation of alkyl chlorides, reducing the efficiency of halogen exchange.

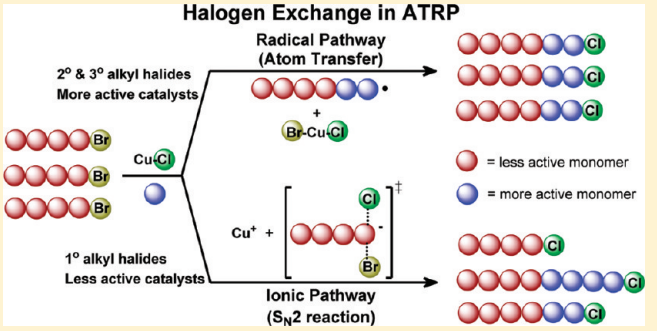

INTRODUCTION

Block copolymers find many applications such as adhesives,[1,2] sealants,[3,4] and surfactants.[5,6] Synthesis of block copolymers is an important procedure for controlled radical polymerization (CRP). Normally, during the synthesis of block copolymers, more active monomers are polymerized before less active monomers to ensure a near simultaneous growth of the second block from the first macroinitiator. This order is generally followed in CRP and, specifically in atom transfer radical polymerization (ATRP), shows that the following order of activity: acrylonitrile > methacrylates > styrene ∼ acrylates > acrylamides ≫ vinyl chloride > vinyl acetate.[7,8] If the order is reversed, the initially extended chains, which have a faster reactivation, would grow more rapidly than the unextended chains, producing polymers with a broad or bimodal molecular weight distribution, as shown in Scheme 1A. However, in ATRP, a procedure known as halogen exchange (HE) allows this order to be altered.[7,9,10] In this technique, a macromolecular alkyl bromide is chain extended with a more reactive monomer in the presence of a $Cu^{(I)}(L)Cl$ catalyst. Since the ATRP equilibrium constant for a chloro-(macro)initiator is ∼1 order magnitude smaller than for a bromo-(macro)initiator,[8] the C−Cl bond formed upon deactivation of the chain extended radical is reactivated more slowly than the remaining bromo-(macro)initiator chain ends. The rate of chain growth of the second block is thus decreased, leading to increased initiation efficiency from the bromo-(macro)initiator and to polymers with a low polydispersity, as shown in Scheme 1B. This technique has been used to chain extend poly(methyl acrylate) macroinitiators with methyl methacrylate to form block copolymers.[10]

Atom transfer radical polymerization is a well-established technique for the synthesis of homo- and block copolymers with defined compositions, architectures, and functionalities.[7,11−16] The ATRP equilibrium (Scheme 2) regulates the control over polymerization and is dominated by the carbon−halogen bond (P_m−X) homolysis, the redox reaction between two oxidation states of the transition metal complexes, and the formation of a copper−halogen bond (X−$Cu^{(II)}$). Altering the halogen atom at the dormant chain end can shift the ATRP equilibrium and affect the kinetics of ATRP process.[9,10,17−24] The weakly associated halide anion (Y) in $Cu^{(I)}(L)Y$ and X−$Cu^{(II)}(L)Y$ species could participate in a S_N2 reaction with alkyl halide (ATRP initiator) during the block copolymer synthesis by halide exchange. Since it would form less active alkyl halide before the more active monomer is added, the benefit of halogen exchange could be lost.

Herein, kinetic parameters of the radical pathway (atom transfer) and ionic pathway (S_N2 reaction) recognized as potential contributors to the halogen exchange process were measured for catalyst complexes formed with three ligands with seven initiators (Scheme 3). This systematic analysis provides an in-depth understanding of the mechanism of HE process and a guide to improve the synthesis of block copolymers by ATRP.

Received: May 6, 2011
Revised: August 15, 2011
Published: September 14, 2011

Scheme 1. Chain Extension from Terminally Functionalized Polymers Composed of Less Active Monomers with a More Active Monomer: (A) Using Regular ATRP; (B) Using ATRP with Halogen Exchange

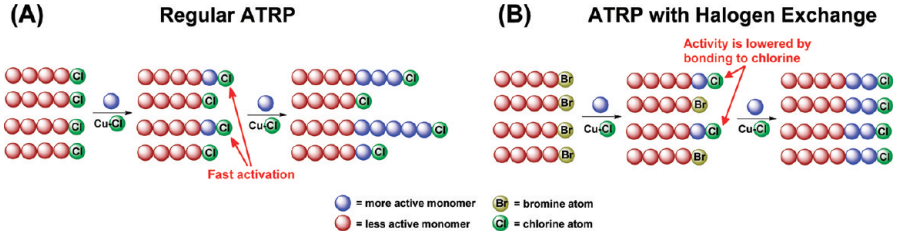

Scheme 2. ATRP Equilibrium between an Alkyl Halide and Copper Complex in the Lower Oxidation State and Alkyl Radical and Copper Complex in the Higher Oxidation State

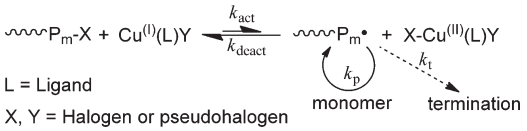

RESULTS AND DISCUSSION

Scheme 4 shows the halogen exchange occurring by both the radical pathway and the ionic pathway. The radical pathway, shown in Scheme 4B, is an atom transfer process based on the accepted ATRP mechanism. Three distinct steps—activation, halogen interchange on the resulting $Cu^{(II)}$ species, and deactivation—are involved in this pathway. Because the rate of activation is generally slower than the rate of halogen interchange and deactivation, the activation step should be the rate-determining step. Therefore, the activation rate constant (k_{act}) measured by trapping experiment with TEMPO[25] has been used to evaluate the contribution of the radical pathway to the overall halogen exchange process.

The ionic pathway, shown in Scheme 4C, is based on the S_N2 mechanism, and this pathway can be termed as a halide exchange. In this pathway the bromo-(macro)initiator can be directly converted to the chloro-(macro)initiator without generation of a radical and before potential addition of the less active monomer. This would result in a diminished level of control in the synthesis of block copolymers. The rate constant of ionic pathway (k_{ionic}) determined in the reaction with NBu_4Cl has been used to evaluate the contribution of the ionic pathway to the overall halogen exchange process. Although halogen exchange can be performed with several copper(I) halides and copper(I) pseudohalides, $Cu^{(I)}$(L)Cl and bromo-initiators were used for the mechanistic study reported in this article.

Radical Pathway (Atom Transfer). The rate-determining step of the radical pathway should be the activation process; therefore, the activation rate constants (k_{act}) were independently determined by UV−vis−NIR spectroscopy using trapping experiments with TEMPO. The radicals generated by C−X bond homolysis from the alkyl halides activated by $Cu^{(I)}$(L)X species are irreversibly trapped by this stable nitroxide radical to yield the corresponding alkoxyamines (Scheme 5). This method was reported before[26] and frequently used to measure the k_{act} in ATRP. Previous studies indicate that TEMPO only performs as a radical trap, and the measured rate constants were independent of the concentration of excess TEMPO.[25,27−31] The kinetic experiments were performed under pseudo-first-order conditions using a large excess of the alkyl halide and nitroxide. The reactions were monitored by following the increase of the UV−vis absorbance at λ_{max} of the formed $Cu^{(II)}$ complexes (λ = 740 nm, ε = 178 L mol^{-1} cm^{-1} for $Cu^{(II)}(bpy)_2X_2$; λ = 740 nm, ε = 220 L mol^{-1} cm^{-1} for $Cu^{(II)}$(PMDETA)X_2; λ = 950 nm, ε = 200 L mol^{-1} cm^{-1} for $Cu^{(II)}$(TPMA)X_2 in acetonitrile). Pseudo-first-order rate constants were obtained from the exponential increase in the UV−vis absorbance by fitting the single exponential $y = A[1 - \exp(-k_{obs}t)] + C$ to the observed time-dependent $Cu^{(II)}$ absorbance. The activation rate constants (k_{act}) were then obtained from $k_{act} = k_{obs}/[\text{alkyl halide}]$.[25] Figure 1 shows a typical experiment for the measurement of k_{act} for $Cu^{(I)}$(PMDETA)Cl with MBriB. All other k_{act} measurements are presented in the Supporting Information (Figures SI 1−12).

The activation rate constants with $Cu^{(I)}$(L)Cl species (k_{act}^{CuCl}) have not been as extensively studied as those with $Cu^{(I)}$(L)Br (k_{act}^{CuBr}).[25,29−32] According to the ATRP mechanism (Scheme 2), the halide counterion is not involved in the activation step, and thus replacing the halide anion in Cu catalysts from Br^- to Cl^- may not affect the value of k_{act} very strongly. This assumption was confirmed by the measurement of k_{act} for selected $Cu^{(I)}$(L)Cl transition metal complexes with a range of initiators (Table 1). The values of k_{act} for selected $Cu^{(I)}$(L)Cl and different initiators are similar to those for corresponding $Cu^{(I)}$(L)Br catalyst complexes. Nevertheless, according to recent speciation studies, halide anions associate reversibly with copper complexes and may affect their reactivities.[33]

Figure 2 shows the similarity of k_{act} for $Cu^{(I)}$(L)Cl and $Cu^{(I)}$(L)Br with PMDETA (Figure 2A) and bpy (Figure 2B) as ligands. The values for k_{act} for the $Cu^{(I)}$(TPMA)Cl complex are too large to be measured by the method used in this study; therefore, only one initiator was selected to confirm the equivalence of k_{act}^{CuCl} and k_{act}^{CuBr}. The values of k_{act}^{CuCl} measured with alkyl chloride are similar to those of k_{act}^{CuBr}, indicating both alkyl halides are activated by the catalyst with a similar role. Because k_{act} of $Cu^{(I)}$(L)Cl is essentially equal to that of $Cu^{(I)}$(L)Br, thus the previously published k_{act} for $Cu^{(I)}$(L)Br species[25,31] can be adopted for the halogen exchange study. As k_{HE} and k_{ionic} were measured at 27 °C, k_{act} for 27 °C (Figure 3) was calculated using the values of k_{act} at 22 °C and the Eyring plot ($\ln(k_{act}/T) = a(1/T) + b$).[25,31]

To better illustrate the trend of the rate constants, different colors and symbols were used to label the data points in the figures. Black, blue, and red symbols represent the rate constants with primary, secondary, and tertiary alkyl halides, respectively;

dx.doi.org/10.1021/ma201035u |Macromolecules 2011, 44, 7546–7557

Scheme 3. Structures of (A) Ligands and (B) Initiators Used in This Kinetic Study of Halogen Exchange in ATRP

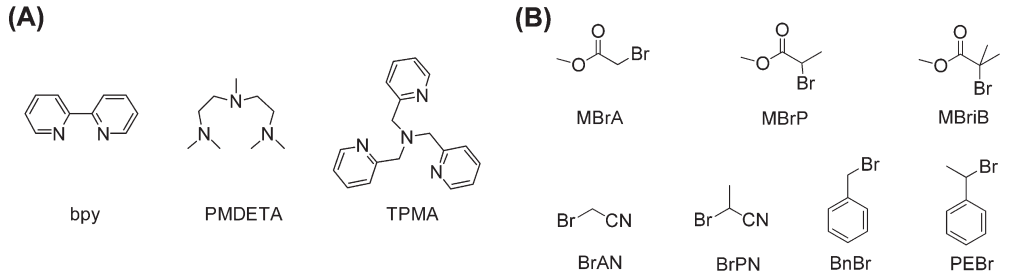

Scheme 4. Proposed Radical and Ionic Pathways in Halogen Exchange Process: (A) Overall Halogen Exchange; (B) Radical Pathway; (C) Ionic Pathway

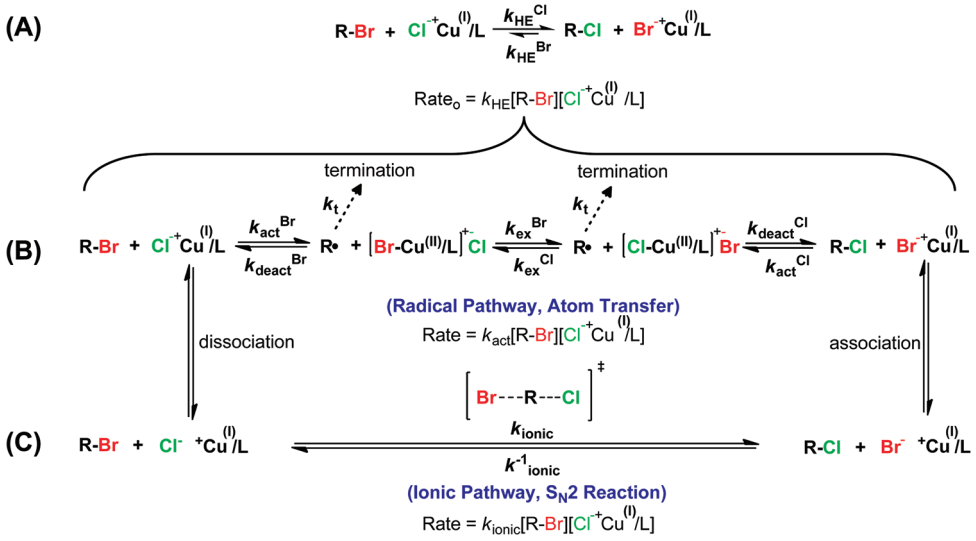

Scheme 5. Schematic Illustration of the Activation Rate Constant (k_{act}) Measurement by Irreversible Trapping of the Formed Radicals with TEMPO

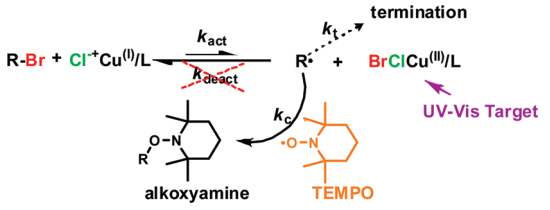

square, triangle, and circle mean the rate constants with ester-, phenyl-, and cyano-initiators, respectively.

The range of ATRP activation rate constants is wide, spanning ~6 orders of magnitude (4.9×10^{-4}–3.6×10^{2} M^{-1} s^{-1}). The values are mainly affected by the ligand associated with the $Cu^{(I)}$ catalysts and the functional group attached to the carbon atom of the C–X bond in the initiators.[29−31] With the same initiator, the ratio of k_{act} with TPMA/PMDETA/bpy is ~1000/50/1 (Figure 3, k_{act}(TPMA) ~ 1000 × k_{act}(bpy); k_{act}(PMDETA) ~ 50 × k_{act}(bpy)) because a ligand, which can better stabilize the $Cu^{(II)}$ state of the catalyst and has a smaller entropic penalty for ligand rearrangement when transitioning from the $Cu^{(I)}$ to $Cu^{(II)}$ state,

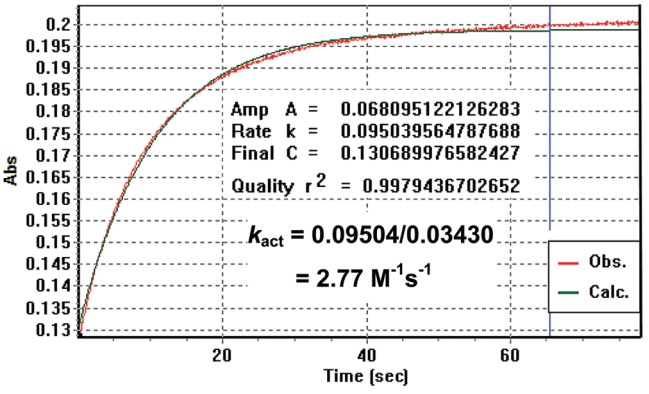

Figure 1. Exponential increase of the absorbance at 950 nm (red line) and the fitting curve (green line) of the reaction of $Cu^{(I)}$(PMDETA)Cl (1.09×10^{-3} mol L^{-1}) with MBriB (3.43×10^{-2} mol L^{-1}) and TEMPO (1.26×10^{-2} mol L^{-1}) in MeCN at 27 °C.

forms the $Cu^{(I)}$ catalyst with higher activity. For the same $Cu^{(I)}$ catalyst, initiators with a cyano functional group have a much larger k_{act} than those with a phenyl or an ester group, following the combination of polar and resonance effects. The influence of a steric effect was also observed and shows the following trend: k_{act}

dx.doi.org/10.1021/ma201035u |Macromolecules 2011, 44, 7546–7557

(tertiary initiators) > k_{act} (secondary initiators) > k_{act} (primary initiators). However, compared to the differences caused by the functional groups, the steric effect has a relatively smaller impact.[7]

Ionic Pathway (Halide Exchange). Weakly associated halides in copper complexes can participate in S_N2 reaction to displace the halides from the initiators via an ionic pathway, concurrently to atom transfer during the halogen exchange. In order to evaluate the contribution of ionic pathway, the halide exchange reaction between tetra-*n*-butylammonium chloride (NBu_4Cl) and alkyl bromides was studied. Tetra-*n*-butylammonium chloride, which dissociates well in polar media,[34] was used as the chloride source to react with equivalent amounts of alkyl bromides (Scheme 6) in order to determine the rate constants for an ionic pathway (k_{ionic}). ^{1}H NMR was used to follow the increase in the alkyl chloride concentration and the decrease in alkyl bromide concentration in the reactions of NBu_4Cl for different initiators. The value for k_{ionic} was measured as the slope of the second-order kinetic plots. Since alkyl chlorides are generally much less reactive than corresponding alkyl bromides,[8] integrated rate law for an irreversible second-order reaction was used though the kinetic order of halide exchange has not firmly been established. A specific example measuring k_{ionic} for the reaction of NBu_4Cl with PEBr is shown in Figure 4. The kinetic plots used to determine the other k_{ionic} are in the Supporting Information (Figures SI 13−19).

The range of k_{ionic} values with NBu_4Cl is from 9.7×10^{-6} to 5.8×10^{-1} M^{-1} s^{-1} (Figure 5). Unlike the activation rate constants, steric effects dominate the behavior of k_{ionic}. The trend of k_{ionic} is (primary initiators) > k_{ionic} (secondary initiators) > k_{ionic} (tertiary initiators) and matches the proposed S_N2 mechanism. The ester-initiators show a higher k_{ionic} than phenyl- and cyano-initiators, but the influence of adjacent functional groups is relatively small.

The rate constants for the ionic pathway (halide exchange), k_{ionic}, of the $Cu^{(II)}(L)Cl_2$ complexes (L = TPMA, PMDETA, bpy) were evaluated by the same method as above and show the same trend as k_{ionic} of NBu_4Cl, in agreement with S_N2 mechanism (Figure 6). The kinetic plots used to determine the k_{ionic} are in the Supporting Information (Figures SI 20−40). Previous studies demonstrated that one chloride in $Cu^{(II)}(L)Cl_2$ complex is directly bonded to the $Cu^{(II)}$ center by a Cu−Cl bond, but the second chloride is not directly coordinated.[35,36] This weakly bonded chloride could dissociate to start the halide exchange

Table 1. Activation Rate Constants (k_{act}) for Selected $Cu^{(I)}$-(L)Cl Species (k_{act}^{CuCl}) with Various Initiators in MeCN at 22 °C and the Corresponding k_{act} for $Cu^{(I)}(L)Br$ (k_{act}^{CuBr})

entry	L	initiator	k_{act}^{CuBr} (M^{-1} s^{-1})[a]	k_{act}^{CuCl} (M^{-1} s^{-1})[b]
1	TPMA	PECl	1.2×10^{-1}	2.0×10^{-1}
2	PMDETA	ClAN	7.1×10^{-2}	6.3×10^{-2}
3	PMDETA	BrAN	3.9	3.9
4	PMDETA	MBrA	1.6×10^{-2}	1.4×10^{-2}
5	PMDETA	MBrP	1.3×10^{-1}	1.8×10^{-1}
6	PMDETA	MBriB	2.4	2.8
7	PMDETA	EtBriB	1.8	2.0
8	bpy	BnBr	1.2×10^{-3}	1.0×10^{-3}
9	bpy	BrAN	8.7×10^{-2}	8.5×10^{-2}
10	bpy	MBrP	4.0×10^{-3}	5.1×10^{-3}
11	bpy	BrPN	2.8×10^{-1}	2.2×10^{-1}
12	bpy	MBriB	3.2×10^{-2}	5.5×10^{-2}

[a] Values from refs 25 and 29−31. [b] $[CuCl]_0/[L]_0/[initiator]_0$ = 2.74 mM/2.74 mM/59.96 mM (entry 1); 2.83 mM/2.83 mM/50.99 mM (entry 2); 1.11 mM/1.11 mM/34.56 mM (entry 3); 2.55 mM/2.56 mM/48.59 mM (entry 4); 2.55 mM/2.56 mM/50.57 mM (entry 5);1.09 mM/1.09 mM/34.30 mM (entry 6); 1.09 mM/1.09 mM/35.34 mM (entry 7); 9.70 mM/19.50 mM/296.29 mM (entry 8); 4.49 mM/9.00 mM/90.46 mM (entry 9); 2.73 mM/5.44 mM/54.64 mM (entry 10); 3.31 mM/6.65 mM/65.84 mM (entry 11); 4.68 mM/9.40 mM/96.12 mM (entry 12). Figures SI 1−12.

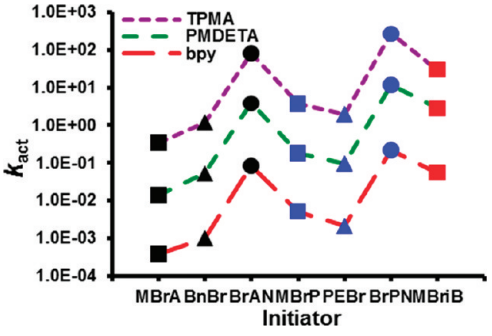

Figure 3. Activation rate constants (k_{act}) for a variety of catalyst complexes and initiators in MeCN at 27 °C. The values of k_{act} are shown in Tables 2−4.

Scheme 6. Model Reaction and the Rate Equation for k_{ionic} Measurement

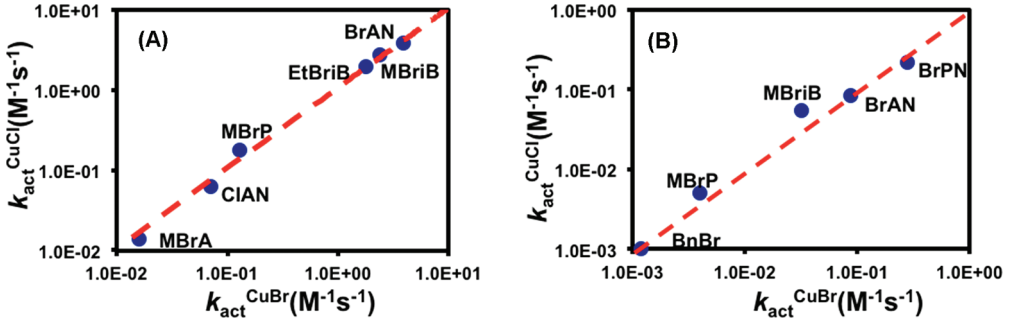

Figure 2. Plots of activation rate constants measured with $Cu^{(I)}(L)Cl$ vs $Cu^{(I)}(L)Br$ in MeCN at 22 °C: (A) L = PMDETA; (B) L = bpy. The values and conditions are shown in Table 1. The dashed line is the calculated line for $k_{act}^{CuCl} = k_{act}^{CuBr}$.

dx.doi.org/10.1021/ma201035u |*Macromolecules* 2011, 44, 7546–7557

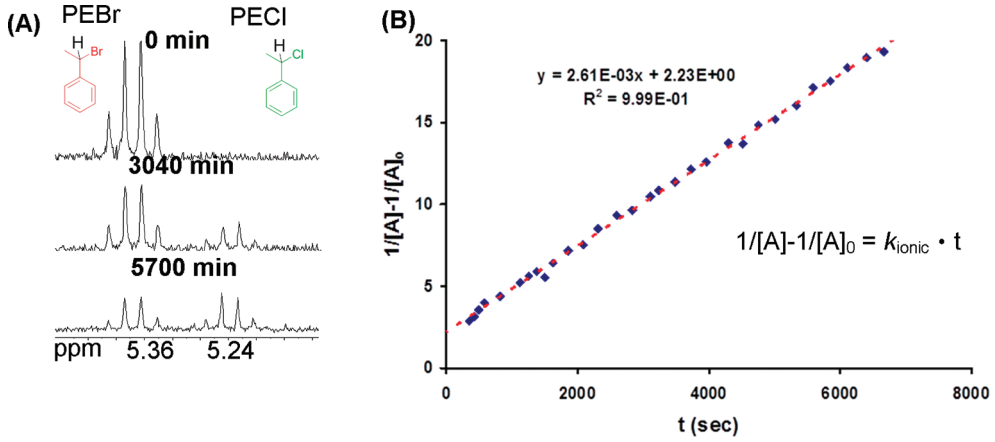

Figure 4. Measurement of the rate constant for an ionic pathway (k_{ionic}) with NBu_4Cl (2.05×10^{-2} M) and PEBr (2.05×10^{-2} M) in MeCN-d_3 at 27 °C: (A) time evolution ^{1}H NMR spectra showing the conversion from PEBr to PECl; (B) second-order kinetic plots used to calculate the value of k_{ionic} for PEBr, $k_{ionic} = 2.61 \times 10^{-3}$ M^{-1} s^{-1}.

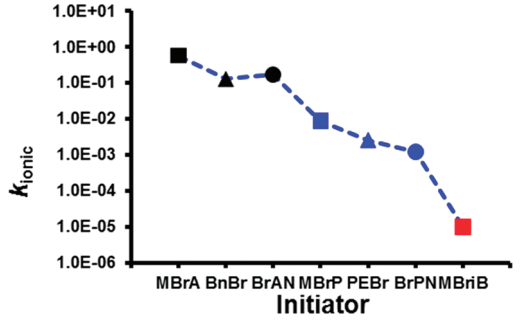

Figure 5. Rate constants for the ionic pathway (k_{ionic}) with NBu_4Cl in MeCN at 27 °C. The values of k_{ionic} are shown in Tables 2−4, and the conditions are shown in the Supporting Information (Figures SI 13−19).

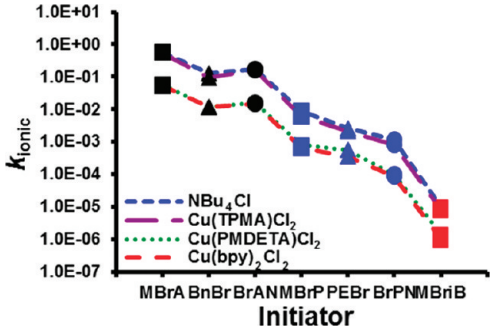

Figure 6. Rate constants of halide exchange (k_{ionic}) in MeCN at 27 °C with NBu_4Cl, $Cu^{(II)}(TPMA)Cl_2$, $Cu^{(II)}(PMDETA)Cl_2$, and $Cu^{(II)}(bpy)_2Cl_2$ versus initiator. The values of k_{ionic} are shown in Table 5, and the conditions are in Figures SI 13−40.

process. The values of k_{ionic} for $Cu^{(II)}(TPMA)Cl_2$ are very close to those for NBu_4Cl which indicate that one chloride in $Cu^{(II)}(TPMA)Cl_2$ complex is almost as dissociated as that in NBu_4Cl. The value for k_{ionic} of the $Cu^{(II)}(PMDETA)Cl_2$ complex are smaller than those for $Cu^{(II)}(TPMA)Cl_2$ and only slightly larger than k_{ionic} value of $Cu^{(II)}(bpy)_2Cl_2$. The smaller values for k_{ionic} mean that the degree of association between $[Cu^{(II)}(L)Cl]^+$ and Cl^- occurs to a greater extent. The ratio of $k_{ionic}(Cu^{(II)}(TPMA)Cl_2)/k_{ionic}(Cu^{(II)}(PMDETA)Cl_2)/k_{ionic}(Cu^{(II)}(bpy)_2Cl_2)$ = 8.6/1.3/1.0 was observed.

Scheme 7. Model Reaction and the Rate Equation for k_{HE} Measurement

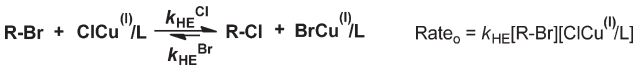

Halogen Exchange. The rate constants of overall halogen exchange, denoted k_{HE}, were measured by following the decrease of the concentration of the alkyl bromide and increase of the concentration of alkyl chloride. In these experiments, alkyl bromides were reacted with 1 equiv of $Cu^{(I)}(L)Cl$ (L = bpy, PMDETA, TPMA) (Scheme 7), and the reaction was monitored using ^{1}H NMR spectra. The slope of the second-order kinetic plots provides the value for k_{HE}. A specific example of determining the k_{HE} for reaction between $Cu^{(I)}(bpy)_2Cl$ and MBrA is shown in Figure 7. All other details of the measurements of k_{HE} can be found in the Supporting Information (Figures SI 41−61).

The values of halogen exchange rate constants, k_{HE}, were largest with $Cu^{(I)}(TPMA)Cl$, followed by $Cu^{(I)}(PMDETA)Cl$, and the k_{HE} with $Cu^{(I)}(bpy)_2Cl$ were the smallest (Figure 8). This trend is similar to that reported for the activation rate constants, k_{act}, and can be correlated with ATRP activity. However, the trend for the same catalysts ($Cu^{(I)}(PMDETA)Cl$, $Cu^{(I)}(bpy)_2Cl$) are somehow different than that for k_{act}, indicating some contributions of ionic pathway.

A more comprehensive analysis of the trend for overall k_{HE} was performed by overlapping the k_{HE} and k_{act} for the same catalyst with the value of k_{ionic} for NBu_4Cl (Figures 9−11). In the halogen exchange reaction of $Cu^{(I)}(bpy)_2Cl$ complex with different initiators, the k_{HE} of secondary and tertiary initiators show a similar trend to that of k_{act}, but the trend for k_{HE} with primary initiators is similar to that for k_{ionic} (Figure 9). This observation indicates that the halogen exchange of $Cu^{(I)}(bpy)_2Cl$ with secondary and tertiary initiators is dominated by the radical pathway, while the ionic pathway dominates the overall halogen exchange with primary initiators. The switch of dominant pathways for the halogen exchange process is due to

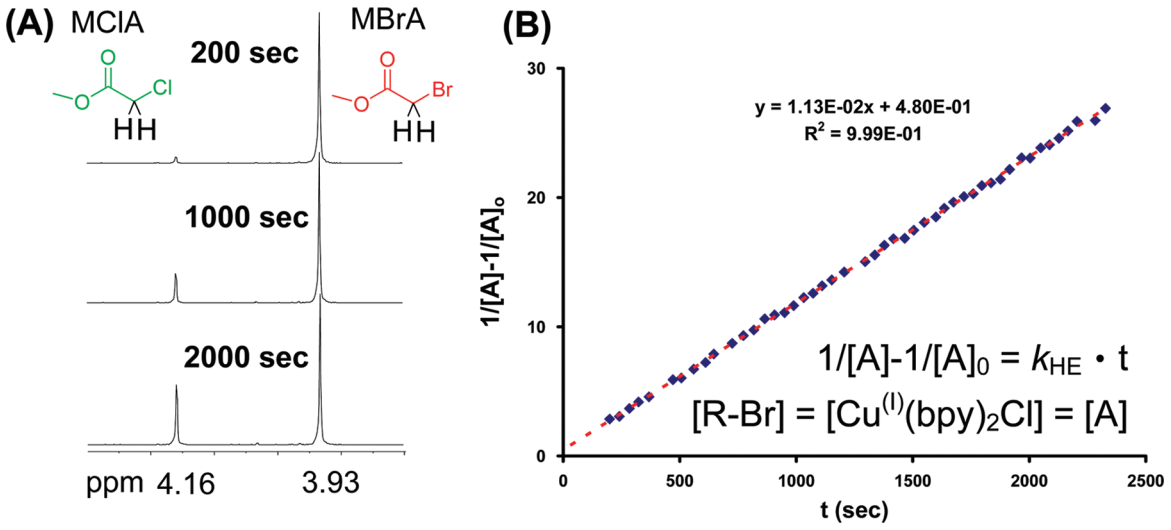

Figure 7. Measurement of rate constants of halogen exchange (k_{HE}) with $Cu^{(I)}(bpy)_2Cl$ (1.98×10^{-2} M) and MBrA (1.98×10^{-2} M) in MeCN-d_3 at 27 °C: (A) time evolution the ^1H NMR spectra showing the conversion from MBrA to MClA; (B) second-order kinetic plots used to calculate the k_{HE} of MBrA, $k_{HE} = 1.13 \times 10^{-2}$ M^{-1} s^{-1}.

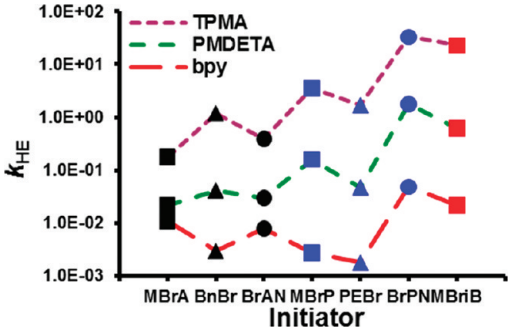

Figure 8. Rate constants for halogen exchange (k_{HE}) in MeCN at 27 °C. The values for k_{HE} are shown in Tables 2−4, and the conditions are shown in the Supporting Information (Figures SI 41−61).

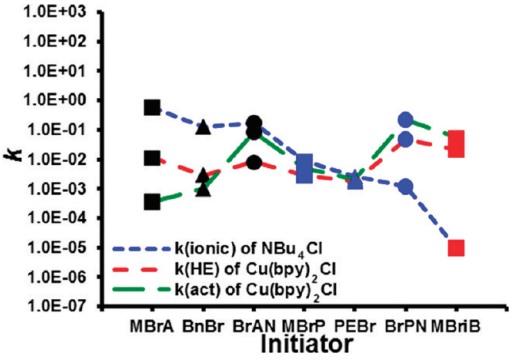

Figure 9. Plots of k_{HE} and k_{act} for $Cu^{(I)}(bpy)_2Cl$ overlapped with k_{ionic} for reaction with NBu_4Cl in MeCN at 27 °C. The values of k_{HE}, k_{ionic}, and k_{act} are shown in Tables 2−4.

the large difference between k_{act} and k_{ionic} for primary initiators ($k_{ionic} \gg k_{act}$).

In the halogen exchange reaction using $Cu^{(I)}(PMDETA)Cl$ (Figure 10) and $Cu^{(I)}(TPMA)Cl$ (Figure 11), the contribution from the radical pathway becomes larger due to an

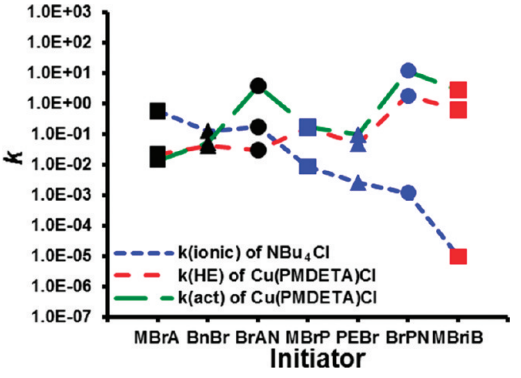

Figure 10. Plots of k_{HE} and k_{act} for $Cu^{(I)}(PMDETA)Cl$ overlapped with k_{ionic} for NBu_4Cl in MeCN at 27 °C. The values of k_{HE}, k_{ionic}, and k_{act} are shown in Tables 2−4.

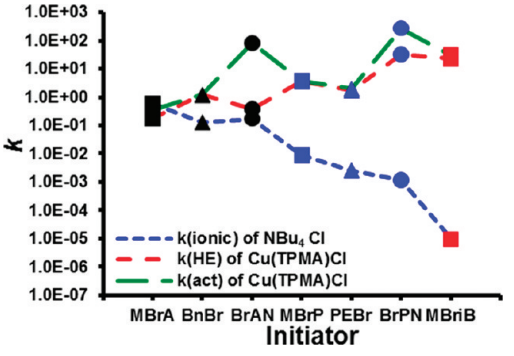

Figure 11. Plots of k_{HE} and k_{act} for $Cu^{(I)}(TPMA)Cl$ with different initiators overlapped with k_{ionic} for NBu_4Cl in MeCN at 27 °C. The values of k_{HE}, k_{ionic}, and k_{act} are shown in Tables 2−4.

increased k_{act}, the ionic pathway becomes less significant. Consequently, the trend for k_{HE} is similar to that for k_{act} with all initiators, with the exception of BrAN. The k_{HE} of BrAN is

dx.doi.org/10.1021/ma201035u |*Macromolecules* 2011, 44, 7546–7557

Table 2. Summary of k_{HE} and k_{act} for $Cu^{(I)}(bpy)_2Cl$ and k_{ionic} for NBu_4Cl in MeCN at 27 °C with the Linear Combination of $k_{HE} = \alpha^{(I)}{}_L k_{ionic} + \beta^{(I)}{}_L k_{act}$

	$k_{HE} = \alpha^{(I)}{}_{bpy} k_{ionic} + \beta^{(I)}{}_{bpy} k_{act}$						
$Cu^{(I)}(bpy)_2Cl$ initiator	k_{HE}	$\alpha^{(I)}{}_{bpy}$	$k_{ionic}(N(Bu)_4Cl)$	$\beta^{(I)}{}_{bpy}$[a]	k_{act}	% ionic[b]	% radical[c]
MBrA	1.1×10^{-2}	1.9×10^{-2}	5.8×10^{-1}	3.2×10^{-1}	4.9×10^{-4}	98.60	1.40
BnBr	3.0×10^{-3}	1.9×10^{-2}	1.3×10^{-1}	4.3×10^{-1}	1.3×10^{-3}	81.03	18.97
BrAN	8.0×10^{-3}	1.9×10^{-2}	1.7×10^{-1}	4.3×10^{-2}	1.1×10^{-1}	39.74	60.26
MBrP	2.8×10^{-3}	1.9×10^{-2}	8.7×10^{-3}	3.9×10^{-1}	6.7×10^{-3}	5.81	94.19
PEBr	1.8×10^{-3}	1.9×10^{-2}	2.6×10^{-3}	6.4×10^{-1}	2.8×10^{-3}	2.70	97.30
BrPN	4.9×10^{-2}	1.9×10^{-2}	1.2×10^{-3}	1.7×10^{-1}	2.9×10^{-1}	0.05	99.95
MBriB	2.2×10^{-2}	1.9×10^{-2}	9.7×10^{-6}	3.0×10^{-1}	7.2×10^{-2}	0.01>	>99.99

[a] Average β value with $Cu^{(I)}(bpy)_2Cl$ is 4.2×10^{-1} excluding β values of BrAN and BrPN. [b] % ionic = $\alpha^{(I)}{}_L \times k_{ionic}(NBu_4Cl)/k_{HE}$. [c] % radical = $\beta^{(I)}{}_L \times k_{act}/k_{HE}$.

Table 3. Summary of k_{HE} and k_{act} for $Cu^{(I)}(PMDETA)Cl$ and k_{ionic} for NBu_4Cl in MeCN at 27 °C with the Linear Combination of $k_{HE} = \alpha^{(I)}{}_L k_{ionic} + \beta^{(I)}{}_L k_{act}$

	$k_{HE} = \alpha^{(I)}{}_{PMDETA} k_{ionic} + \beta^{(I)}{}_{PMDETA} k_{act}$						
$Cu^{(I)}(PMDETA)Cl$ initiator	k_{HE}	$\alpha^{(I)}{}_{PMDETA}$	$k_{ionic}(N(Bu)_4Cl)$	$\beta^{(I)}{}_{PMDETA}$[a]	k_{act}	% ionic[b]	% radical[c]
MBrA	2.2×10^{-2}	2.6×10^{-2}	5.8×10^{-1}	3.8×10^{-1}	1.8×10^{-2}	68.55	31.45
BnBr	4.2×10^{-2}	2.6×10^{-2}	1.3×10^{-1}	5.7×10^{-1}	6.8×10^{-2}	8.05	91.95
BrAN	3.0×10^{-2}	2.6×10^{-2}	1.7×10^{-1}	5.1×10^{-3}	5.1	14.73	85.27
MBrP	1.6×10^{-1}	2.6×10^{-2}	8.7×10^{-3}	8.5×10^{-1}	1.9×10^{-1}	0.14	99.86
PEBr	4.8×10^{-2}	2.6×10^{-2}	2.6×10^{-3}	3.5×10^{-1}	1.4×10^{-1}	0.14	99.86
BrPN	1.8	2.6×10^{-2}	1.2×10^{-3}	7.0×10^{-2}	2.6×10^{1}	0.01>	>99.99
MBriB	6.3×10^{-1}	2.6×10^{-2}	9.7×10^{-6}	2.1×10^{-1}	3.1	0.01>	>99.99

[a] Average β value with $Cu^{(I)}(PMDETA)Cl$ is 4.7×10^{-1} excluding β values of BrAN and BrPN. [b] % ionic = $\alpha^{(I)}{}_L \times k_{ionic}(NBu_4Cl)/k_{HE}$. [c] % radical = $\beta^{(I)}{}_L \times k_{act}/k_{HE}$.

Table 4. Summary of k_{HE} and k_{act} for $Cu^{(I)}(TPMA)Cl$ and k_{ionic} for NBu_4Cl in MeCN at 27 °C with the Linear Combination of $k_{HE} = \alpha^{(I)}{}_L k_{ionic} + \beta^{(I)}{}_L k_{act}$

	$k_{HE} = \alpha^{(I)}{}_{TPMA} k_{ionic} + \beta^{(I)}{}_{TPMA} k_{act}$						
$Cu^{(I)}(TPMA)Cl$ initiator	k_{HE}	$\alpha^{(I)}{}_{TPMA}$	$k_{ionic}(N(Bu)_4Cl)$	$\beta^{(I)}{}_{TPMA}$[a]	k_{act}	% ionic[b]	% radical[c]
MBrA	1.8×10^{-1}	1.5×10^{-1}	5.8×10^{-1}	2.0×10^{-1}	4.6×10^{-1}	48.33	51.67
BnBr	1.2	1.5×10^{-1}	1.3×10^{-1}	7.5×10^{-1}	1.6	1.63	98.38
BrAN	3.9×10^{-1}	1.5×10^{-1}	1.7×10^{-1}	3.4×10^{-3}	1.1×10^{2}	6.54	93.46
MBrP	3.6	1.5×10^{-1}	8.7×10^{-3}	7.2×10^{-1}	5.0	0.04	99.96
PEBr	1.7	1.5×10^{-1}	2.6×10^{-3}	6.5×10^{-1}	2.6	0.02	99.98
BrPN	3.3×10^{1}	1.5×10^{-1}	1.2×10^{-3}	9.3×10^{-2}	3.6×10^{2}	0.01>	>99.99
MBriB	2.3×10^{1}	1.5×10^{-1}	9.7×10^{-6}	5.8×10^{-1}	3.9×10^{1}	0.01>	>99.99

[a] Average β value with $Cu^{(I)}(TPMA)Cl$ is 5.8×10^{-1} excluding β values of BrAN and BrPN. [b] % ionic = $\alpha^{(I)}{}_L \times k_{ionic}(NBu_4Cl)/k_{HE}$. [c] % radical = $\beta^{(I)}{}_L \times k_{act}/k_{HE}$.

surprisingly smaller than k_{act}, in comparison to other initiators. This is possibly caused by either the reduction of radical to carbanion or radical termination reactions. In addition, the difference between k_{HE} and k_{act} progressively decreases from $Cu^{(I)}(bpy)_2Cl$ to $Cu^{(I)}(PMDETA)Cl$ and to $Cu^{(I)}(TPMA)Cl$, indicating that the efficiency of halogen exchange can be improved by using more active catalysts.

The contributions of both the radical atom transfer and ionic halide exchange to the overall halogen exchange were evaluated using a linear combination equation: $k_{HE} = \alpha^{(I)}{}_L k_{ionic} + \beta^{(I)}{}_L k_{act}$, since the observed halogen exchange should be the sum of contributions from these two independent pathways. The superscript (I) refers to $Cu^{(I)}$ species. The values α and β show how much the halide exchange in the presence of $Cu^{(I)}Cl$ species is slower in comparison with NBu_4Cl and how much halogen exchange is slower that a pure activation step, respectively. The results are listed in Tables 2, 3, and 4 for $Cu^{(I)}(bpy)_2Cl$, $Cu^{(I)}$-(PMDETA)Cl, and $Cu^{(I)}(TPMA)Cl$, respectively.

dx.doi.org/10.1021/ma201035u |*Macromolecules* 2011, 44, 7546–7557

Table 5. Summary of k_{ionic} for $Cu^{(II)}(L)Cl_2$ (L = TPMA, PMDETA, bpy) and NBu_4Cl with Different Initiators in MeCN at 27 °C[a]

initiator	NBu_4Cl	$Cu(TPMA)Cl_2$	$Cu(PMDETA)Cl_2$	$Cu(bpy)_2Cl_2$	$\alpha^{(II)}{}_{TPMA}$	$\alpha^{(II)}{}_{PMDETA}$	$\alpha^{(II)}{}_{bpy}$[b]
MBrA	5.8×10^{-1}	5.5×10^{-1}	5.6×10^{-2}	5.1×10^{-2}	9.5×10^{-1}	9.7×10^{-2}	8.8×10^{-2}
BnBr	1.3×10^{-1}	9.3×10^{-2}	1.2×10^{-2}	1.2×10^{-2}	7.2×10^{-1}	9.2×10^{-2}	9.2×10^{-2}
BrAN	1.7×10^{-1}	1.6×10^{-1}	1.6×10^{-2}	1.5×10^{-2}	9.4×10^{-1}	9.4×10^{-2}	8.8×10^{-2}
MBrP	8.7×10^{-3}	6.1×10^{-3}	7.9×10^{-4}	6.4×10^{-4}	7.0×10^{-1}	9.1×10^{-2}	7.4×10^{-2}
PEBr	2.6×10^{-3}	2.2×10^{-3}	5.8×10^{-4}	3.6×10^{-4}	8.5×10^{-1}	2.2×10^{-1}	1.4×10^{-1}
BrPN	1.2×10^{-3}	8.0×10^{-4}	1.0×10^{-4}	8.8×10^{-5}	6.7×10^{-1}	8.3×10^{-2}	7.3×10^{-2}
MBriB	9.7×10^{-6}	8.1×10^{-6}	1.4×10^{-6}	9.9×10^{-7}	8.4×10^{-1}	1.4×10^{-1}	1.0×10^{-1}

[a] Conditions are in Figures SI 13−40. [b] Because $Cu(L)Cl_2$ does not activate the alkyl halide, k_{act} for $Cu(L)Cl_2$ should be zero, and thus $k_{HE} = k_{ionic}(L) = \alpha^{(II)}{}_L k_{ionic}(NBu_4Cl) + \beta k_{act} = \alpha^{(II)}{}_L k_{ionic}$. Therefore, $\alpha^{(II)}{}_L = k_{ionic}(L)/k_{ionic}(NBu_4Cl)$.

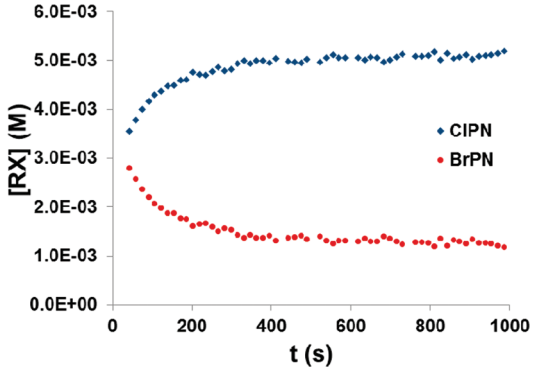

Figure 12. Time-dependent [BrPN] and [ClPN] to estimate the equilibrium constant of halogen exchange (K_{ex}) with $Cu^{(I)}(PMDETA)Cl$ and BrPN in MeCN-d_3 at 27 °C. $[Cu^{(I)}(PMDETA)Cl]_0 = 6.3 \times 10^{-3}$ M; $[BrPN]_0 = 6.3 \times 10^{-3}$ M; $[ClPN]_{eq} = 5.2 \times 10^{-3}$ M; $[BrPN]_{eq} = 1.1 \times 10^{-3}$ M; $K_{ex} = 5.6$.

The values of $\alpha^{(I)}{}_L$ and $\beta^{(I)}{}_L$ were estimated by using the following principles: (1) both $\alpha^{(I)}{}_L$ and $\beta^{(I)}{}_L$ should be larger than 0 and smaller than 1; (2) the value of $\alpha^{(I)}{}_L$ should be identical for all initiators with the same $Cu^{(I)}$ species because the extent of dissociation of chloride from $Cu^{(I)}(L)Cl$ is not affected by the nature of the initiators; (3) the $\alpha^{(I)}{}_L$ value was calculated from the kinetic data for MBrA (k_{HE}, k_{act}, k_{ionic}) because it has the smallest k_{act} and largest k_{ionic}, increasing the accuracy of the value of $\alpha^{(I)}{}_L$; (4) the value of $\beta^{(I)}{}_L$ was then obtained from the equation of $\beta^{(I)}{}_L = (k_{HE} - \alpha^{(I)}{}_L k_{ionic})/k_{act}$ once $\alpha^{(I)}{}_L$ was determined. The values of $\alpha^{(I)}{}_L$ and $\beta^{(I)}{}_L$ were further used to determine the contribution of ionic pathway (% ionic in Tables 2−4) and radical pathway (% radical in Tables 2−4) to the halogen exchange by % ionic = $\alpha^{(I)}{}_L \times k_{ionic}(N(Bu)_4Cl)/k_{HE}$ and % radical = $\beta^{(I)}{}_L \times k_{act}/k_{HE}$, respectively.

The $Cu^{(I)}(bpy)_2Cl$ system is discussed as an example. Since the value of k_{act} for MBrA is quite small (4.9×10^{-4} M^{-1} s^{-1}) and the contribution of the radical pathway, $\beta^{(I)}{}_{bpy}k_{act}$, is also small, the value of $\alpha^{(I)}{}_{bpy}$ can be estimated from $k_{HE} = \alpha^{(I)}{}_{bpy}k_{ionic}$ as 1.90×10^{-2}. The range for the value of $\alpha^{(I)}{}_{bpy}$ was found to be $1.90 \times 10^{-2} > \alpha^{(I)}{}_{bpy} > 1.83 \times 10^{-2}$ in order to obtain a $\beta^{(I)}{}_{bpy}$ value within the range of $0 < \beta^{(I)}{}_{bpy} < 1$. The median value for $\alpha^{(I)}{}_{bpy}$, 1.87×10^{-2}, was used to calculate the $\beta^{(I)}{}_{bpy}$ values for each alkyl halide (Table 2). The range of values for $\alpha^{(I)}{}_{PMDETA}$ with $Cu^{(I)}(PMDETA)Cl$ was $3.8 \times 10^{-2} > \alpha^{(I)}{}_{PMDETA} > 1.4 \times 10^{-2}$, which was larger than that of the $Cu^{(I)}(bpy)_2Cl$ system. The median number for $\alpha^{(I)}{}_{PMDETA}$, 2.6×10^{-2}, was used to calculate the $\beta^{(I)}{}_{PMDETA}$ values for

Scheme 8. Model Reactions and Kinetic Parameters for Predici Simulation of Halogen Exchange

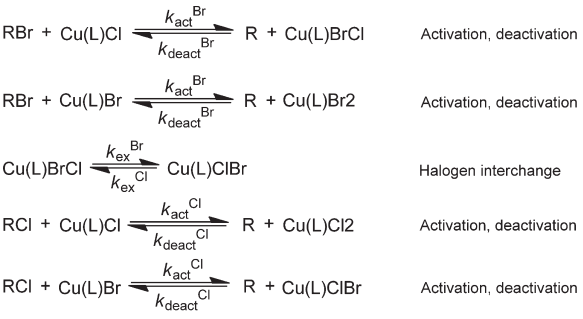

RBr = MBrP; Cu(L)Cl = Cu(PMTEDA)Cl; $[RBr]_o = 5x10^{-3}$ M; $[Cu(L)Cl]_o = 5x10^{-3}$ M

$k_{act}{}^{Br} = 1.7 \times 10^{-1}$ M^{-1} s^{-1}; $k_{deact}{}^{Br} = 4.3 \times 10^{7}$ M^{-1} s^{-1}

$k_{act}{}^{Cl} = 7.8 \times 10^{-3}$ M^{-1} s^{-1}; $k_{deact}{}^{Cl} = 2.4 \times 10^{7}$ M^{-1} s^{-1}

$k_{ex}{}^{Br} = 1.0 \times 10^{6}$ s^{-1}; $k_{ex}{}^{Cl} = 1.8 \times 10^{5}$ s^{-1}; $k_t = 1.0 \times 10^{9}$ M^{-1} s^{-1}

$Cu^{(I)}(PMDETA)Cl$ (Table 3). The range of $\alpha^{(I)}{}_L$ values for $Cu^{(I)}(TPMA)Cl$ was even larger ($3 \times 10^{-1} > \alpha^{(I)}{}_{TPMA} > 0$) since k_{act} is 10 times larger than k_{ionic}, causing difficulties in distinguishing the influence of $\alpha^{(I)}{}_{TPMA}$. In this case the median number, 1.5×10^{-1}, was used for $\beta^{(I)}{}_{TPMA}$ estimation (Table 4). Fortunately, the accuracy of $\beta^{(I)}{}_{TPMA}$ is not significantly affected by the less precise $\alpha^{(I)}{}_{TPMA}$ values because the contribution of the ionic pathway is relatively small.

***α* Values.** The linear combination equation provides information on the relative contribution of the ionic pathway ($\alpha^{(I)}{}_L k_{ionic}/k_{HE}$) and the radical pathway ($\beta^{(I)}{}_L k_{act}/k_{HE}$) to the halogen exchange. Since k_{ionic}, measured with NBu_4Cl, should correspond to the halide exchange rate constant for a fully dissociated chloride, the $\alpha^{(I)}{}_L$ value could be correlated with the degree of dissociation of a chloride ion from the $Cu^{(I)}(L)Cl$ catalysts. The ratio of $\alpha^{(I)}{}_{TPMA}/\alpha^{(I)}{}_{PMDETA}/\alpha^{(I)}{}_{bpy} = 1.5 \times 10^{-1}/2.6 \times 10^{-2}/1.87 \times 10^{-2}$ indicates that the chloride is weakly associated with $[Cu^{(I)}(TPMA)]^+$ but interacts much stronger with $[Cu^{(I)}(bpy)_2]^+$. The association between Cl^- and $Cu^{(I)}(PMDETA)^+$ is similar to that for Cl^- and $[Cu^{(I)}(bpy)_2]^+$. This trend is similar to that observed in the k_{ionic} measurements using $Cu^{(II)}(L)Cl_2$ as a chloride provider (Figure 6 and Table 5).

The trend $\alpha^{(II)}{}_{TPMA}/\alpha^{(II)}{}_{PMDETA}/\alpha^{(II)}{}_{bpy} = 8.1 \times 10^{-1}/1.2 \times 10^{-1}/9.4 \times 10^{-2} = 8.6/1.3/1.0$ is similar to that for

dx.doi.org/10.1021/ma201035u |*Macromolecules* 2011, 44, 7546–7557

$\alpha^{(I)}_{TPMA}/\alpha^{(I)}_{PMDETA}/\alpha^{(I)}_{bpy} = 1.5 \times 10^{-1}/2.6 \times 10^{-2}/1.9 \times 10^{-2} = 8.0/1.4/1.0$. Recent speciation studies, evaluating the stability constants (K) for copper complexes used as catalysts in ATRP, also support these observations.[33]

β Values. The $\beta^{(I)}_{L}$ values define the efficiency of the halogen exchange process via atom transfer. It should be equal to 1.0 for the ideal case when every ATRP activation converts an alkyl bromide to an alkyl chloride. However, due to the reverse reactions (back deactivation to an alkyl bromide and activation of a product alkyl chloride), termination, and side reactions, most of the initiators show $\beta^{(I)}_{L}$ values smaller than 1. Values of β for BrAN are much smaller and indicate side reactions, as discussed previously.

Although the $\beta^{(I)}_{L}$ values for the five benzyl and ester initiators fluctuate, a discernible trend exists. The average $\beta^{(I)}_{L}$ value of $Cu^{(I)}$(TPMA)Cl is the highest (5.8×10^{-1}, Table 4), followed by those of $Cu^{(I)}$(PMDETA)Cl (4.7×10^{-1}, Table 3) and last by $Cu^{(I)}(bpy)_2Cl$ (4.2×10^{-1}, Table 2). The small increase of the average $\beta^{(I)}_{L}$ value from $Cu^{(I)}(bpy)_2Cl$ to $Cu^{(I)}$(PMDETA)Cl to $Cu^{(I)}$(TPMA)Cl indicates the efficiency of halogen exchange can be improved by using more active ATRP catalysts.

The contributions of ionic pathway ($\alpha^{(I)}_{L}k_{ionic}/k_{HE}$) and radical pathway ($\beta^{(I)}_{L}k_{act}/k_{HE}$) show a more clear trend: with the same initiators, the contribution of radical pathway increases for more active catalysts ($Cu^{(I)}$(TPMA)Cl > $Cu^{(I)}$(PMDETA)Cl > $Cu^{(I)}(bpy)_2Cl$); with the same catalysts, the contribution of radical pathway follows the trend: tertiary alkyl halides > secondary alkyl halides > primary alkyl halides (Tables 2−4, % radical). Radical pathway has the smallest contribution when MBrA was used but more than 95% contribution with secondary and tertiary alkyl halides, which indicates that more active catalysts and secondary or tertiary initiators are better substrates for the halogen exchange process.

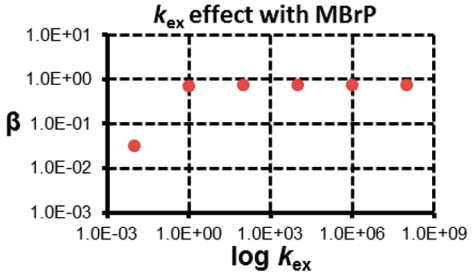

Figure 13. Influence of k_{ex}^{Br} on β values simulated with kinetic parameters for $Cu^{(I)}$(PMDETA)Br and MBrP using the model in Scheme 8. k_{ex}^{Cl} was varied as well to keep K_{ex} constant.

K_{ex} Values. Equilibrium constant of halogen interchange at $Cu^{(II)}$ center (K_{ex}) was estimated by using the $[RBr]_{eq}$ and $[RCl]_{eq}$ in the halogen exchange process together with the reported values of K_{ATRP} for Br and Cl systems (eqs 1−3).[31] Since the radical species ($R^{\bullet}$) is not involved in the halogen exchange on $Cu^{(II)}(L)^{2+}$, K_{ex} should be the same for each initiator. Thus, the halogen exchange of $Cu^{(I)}$(PMDETA)Cl and BrPN was used to estimate K_{ex} of $Cu^{(II)}$(PMDETA)BrCl (Figure 12), since this system reached equilibrium very quickly. Using eq 3 with $K_{ATRP}^{Br} = 5.9 \times 10^{-7}$, $K_{ATRP}^{Cl} = 1.7 \times 10^{-7}$, $[ClPN]_{eq} = 5.2 \times 10^{-3}$ M, and $[BrPN]_{eq} = 1.1 \times 10^{-3}$ M, K_{ex} was calculated as 5.6. Similar values were obtained for other systems. The value $K_{ex} = 5.6$ indicates that Cu^{II}/L species has small preference for bonding with Cl stronger than with Br anion, also in agreement with speciation results.[33]

$$\mathrm{CuCl} + \mathrm{RBr} \underset{}{\overset{K_{ATRP}^{Br}}{\rightleftharpoons}} R^{\bullet} + (\mathrm{Cu{-}Br})\mathrm{Cl} \overset{K_{ex}}{\rightleftharpoons} R^{\bullet} + (\mathrm{Cu{-}Cl})\mathrm{Br} \underset{K_{ATRP}^{Cl}}{\rightleftharpoons} \mathrm{CuBr} + \mathrm{RCl} \quad (1)$$

$$K_{HE} = \frac{[RCl]_{eq}[CuBr]_{eq}}{[RBr]_{eq}[CuCl]_{eq}} = \frac{[RCl]_{eq}^{2}}{[RBr]_{eq}^{2}} = \frac{K_{ATRP}^{Br}K_{ex}}{K_{ATRP}^{Cl}} \quad (2)$$

$$K_{ex} = \frac{K_{ATRP}^{Cl}[RCl]_{eq}^{2}}{K_{ATRP}^{Br}[RBr]_{eq}^{2}} \quad (3)$$

Kinetic Modeling. The influence of activation, deactivation, and termination on β values was evaluated computationally using Predici.[37] Simulations were performed using rate constants for $Cu^{(I)}$(PMDETA)Cl and MBrP available in the literature and comparing them with those obtained in the study. The model reactions and kinetic parameters for halogen exchange are shown in Scheme 8. The following procedure was used to better understand how different parameters affect β values: (1) time-dependent [RBr] and [RCl] were obtained by Predici using various kinetic parameters; (2) conversion was calculated as $[RBr]/([RBr] + [RCl])$; (3) second-order kinetic plots of $1/[RBr] - 1/[RB]_0 = (1/[RBr]_0) \times ((1/\text{conversion}) - 1) = k_{HE} \times t$ provided the values of k_{HE}; (4) β values were calculated as $\beta = k_{HE}/k_{act}^{Br}$.

Initially, in the simulations, the ionic pathway (halide exchange) was neglected to simplify the system because its contribution to overall halogen exchange is very small (0.14% in Table 3). Initial concentrations of Cu(L)Cl and RBr were equal

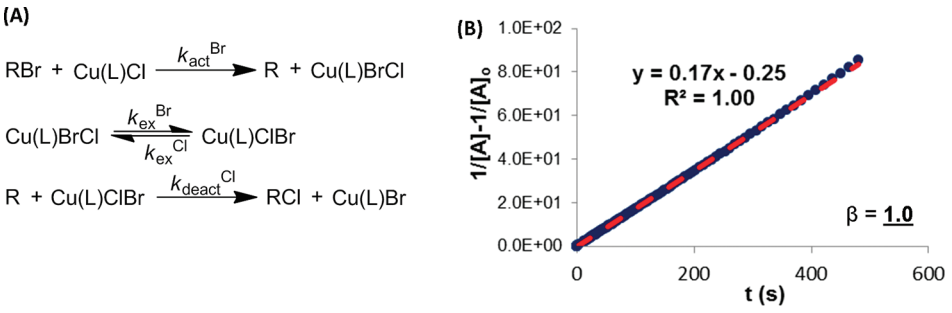

Figure 14. (A) Model in Predici simulation for halogen exchange including only the forward reactions. (B) Second-order kinetic plots of [MBrP] performed by Predici simulation of halogen exchange including only the forward reactions to estimate β value.

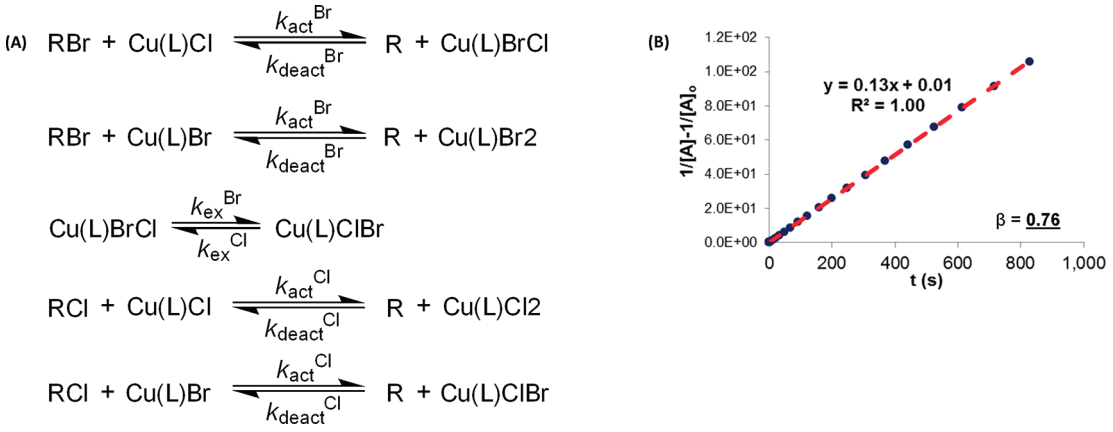

Figure 15. (A) Model in Predici simulation for halogen exchange including only atom transfer mechanism. (B) Second-order kinetic plots of [MBrP] performed by Predici simulation of halogen exchange including only atom transfer mechanism to estimate β value.

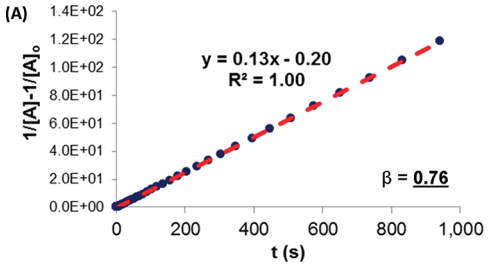

(B)

Reaction	β
Forward Only	1.0
Atom Transfer	0.76
Termination	0.76
Expt. value	0.85

Figure 16. (A) Second-order kinetic plots of [MBrP] performed by Predici simulation of halogen exchange using the model in Scheme 8 to estimate β value. (B) Simulated β values given by different model reactions for the halogen exchange.

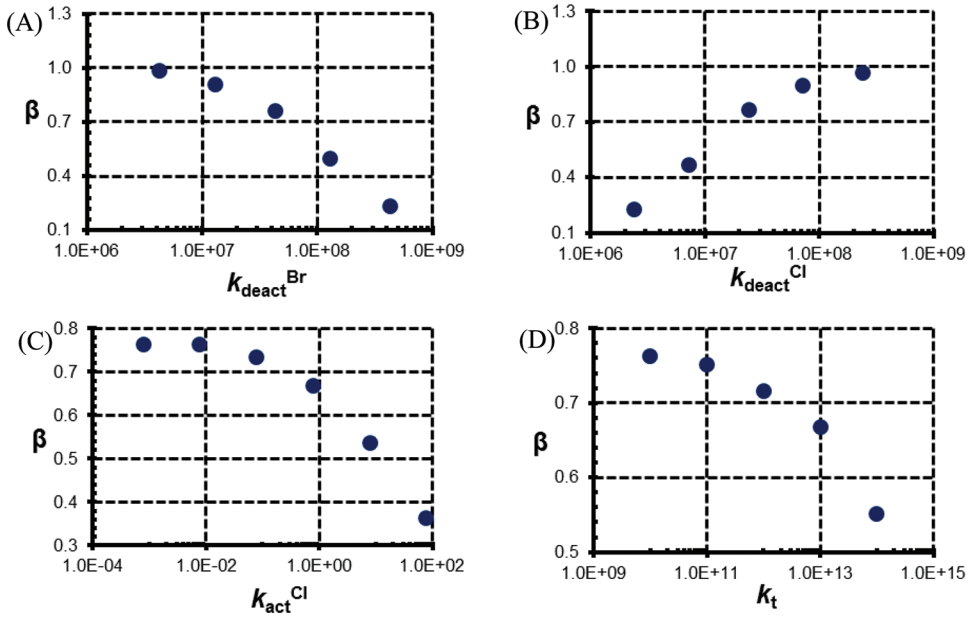

Figure 17. Influence of (A) k_{deact}^{Br}, (B) k_{deact}^{Cl}, (C) k_{act}^{Cl}, and (D) k_t to β value simulated with kinetic parameters for MBrP and model shown in Scheme 8. When one parameter was varied, all other parameters were constant.

to 5×10^{-3} M. The reported activation and deactivation rate constants (k_{act}^{Br}, k_{act}^{Cl}, k_{deact}^{Br}, and k_{deact}^{Cl}) in MeCN at 22 °C[31] were used. The experimental β values were recalculated using k_{act}^{Br} at 22 °C to compare with the simulated ones. A termination rate constant of 1×10^9 M^{-1} s^{-1} was used. The rate constants of halide interchange at $Cu^{(II)}(PMDETA)^{2+}$ were unknown although their ratio was experimentally determined (cf. previous section) as $K_{ex} = k_{ex}^{Br}/k_{ex}^{Cl} = 5.6$. These rate constants were

dx.doi.org/10.1021/ma201035u |*Macromolecules* 2011, 44, 7546–7557

initially assumed as $k_{ex}^{Br} = 1.0 \times 10^6\ s^{-1}$ and $k_{ex}^{Cl} = 1.8 \times 10^5\ s^{-1}$ and then subsequently varied to evaluate their influence on β.

The value of k_{ex}^{Br} was varied from 10^8 to $10^{-2}\ s^{-1}$ with a constant value $K_{ex} = 5.6$ in the simulation using kinetic parameters of MBrP. The β value stayed constant for $k_{ex}^{Br} > 1\ s^{-1}$ but decreased to 3.2×10^{-2} only for $k_{ex}^{Br} = 1 \times 10^{-2}\ s^{-1}$ (Figure 13). The speciation studies[33] indicate the dissociation constants of halides from X−$Cu^{(II)}$/L species in the range K_{dis} ca. 10^{-5}−10^{-6} M. Assuming that association proceeds with the diffusion controlled rate $k_{ass} = 10^9\ M^{-1}\ s^{-1}$, the dissociation should occur with the rate constant $k_{diss} = 10^3$ to $10^4\ s^{-1}$. Of course, the halide exchange at $Cu^{(II)}$ center may occur faster, without full halide dissociation. Regardless, it seems that values of $\beta < 1$ are not caused by slow halide exchange but rather by some other reactions.

The simulations were started from the simplest model in which only the forward reactions of halogen exchange were concerned (Figure 14A). In this case, β value is equal to 1 (Figure 14B), indicating that each activation converts one alkyl bromide to one alkyl chloride irreversibly. However, when the reverse reactions were added (Figure 15A), the β value was decreased from 1 to 0.76 as shown in Figure 15B. Finally, radical termination was included in the simulation (Scheme 8) and caused no further difference to β value (Figure 16A). Simulated β values given by different model reactions are summarized in Figure 16B and are slightly smaller than the experimental value of $\beta = 0.85$ (Table 3). The small difference may also be due to a limited accuracy of previously measured k_{act} and k_{deact} values.

However, some β values in Tables 1−3 are smaller than 0.76, and it was of interest to evaluate how various kinetic parameters can affect β. Therefore, the values of k_{deact}^{Br}, k_{deact}^{Cl}, k_{act}^{Cl}, and k_t were varied one at a time to study the influence of deactivation, activation, and termination on β value (Figure 17). The following trends were observed: (1) the larger k_{deact}^{Br}, the smaller β value (Figure 17A); (2) the larger k_{deact}^{Cl}, which contributes to the generation of alkyl chlorides, gives a larger β value (Figure 17B); (3) the larger k_{act}^{Cl}, which regenerates radical from alkyl chlorides, the smaller β value (Figure 17C); (4) k_t has essentially no effect on the β values in a reasonable range of k_t values. However, when radical termination is significant (e.g., in systems with high K_{ATRP}), β could be affected by termination (Figure 17D); (5) β value is more sensitive to the changes of k_{deact}^{Br} and k_{deact}^{Cl} and less sensitive to the change of k_{act}^{Cl} and k_t.

These simulations indicate that the β value is mainly affected by k_{deact}^{Cl} and k_{deact}^{Br}. The larger k_{deact}^{Cl} and the smaller k_{deact}^{Br} provide a β closer to 1. The values of k_{ex}^{Br} have no effect on β, if they are larger than $1\ s^{-1}$.

SUMMARY

The contributions of a radical pathway (atom transfer) and an ionic pathway (S_N2 reaction) to halogen exchange in ATRP were quantitatively studied for seven alkyl halides and three $Cu^{(I)}$-(L)Cl complexes. Radical pathway dominates the HE process for 3° and 2° alkyl bromides with more active complexes such as $Cu^{(I)}$(TPMA)Cl. Ionic pathway, however, becomes important for 1° alkyl bromides and less active complexes. These studies also revealed that the dissociation of halide anion from $Cu^{(I)}$(L)X and $Cu^{(II)}$(L)X_2 complexes is affected by the structure of copper complexes. In addition, the reverse reactions such as deactivation of alkyl bromides and activation of alkyl chlorides in the radical pathway reduce the efficiency of halogen exchange.

ASSOCIATED CONTENT

Supporting Information. Experimental section, ^1H NMR spectrum of all alkyl halides, and kinetic plots used to evaluate k_{act}, k_{ionic}, and k_{HE}. This material is available free of charge via the Internet at http://pubs.acs.org.

AUTHOR INFORMATION

Corresponding Author
*E-mail: km3b@andrew.cmu.edu.

ACKNOWLEDGMENT

This research was supported by the National Science Foundation (CHE-10-26060) and the members of the CRP Consortium at Carnegie Mellon University.

REFERENCES

(1) Simal, F.; Jeusette, M.; Leclere, P.; Lazzaroni, R.; Roose, P. *J. Adhes. Sci. Technol.* **2007**, *21*, 559–574.
(2) Creton, C.; Hu, G. J.; Deplace, F.; Morgret, L.; Shull, K. R. *Macromolecules* **2009**, *42*, 7605–7615.
(3) Matsui, T.; Miwa, Y. *J. Appl. Polym. Sci.* **1999**, *71*, 59–66.
(4) Nivasu, V. M.; Reddy, T. T.; Tammishetti, S. *Biomaterials* **2004**, *25*, 3283–3291.
(5) Jain, S.; Bates, F. S. *Science* **2003**, *300*, 460–464.
(6) Li, W. W.; Min, K.; Matyjaszewski, K.; Stoffelbach, F.; Charleux, B. *Macromolecules* **2008**, *41*, 6387–6392.
(7) Braunecker, W. A.; Matyjaszewski, K. *Prog. Polym. Sci.* **2007**, *32*, 93–146.
(8) Lin, C. Y.; Coote, M. L.; Gennaro, A.; Matyjaszewski, K. *J. Am. Chem. Soc.* **2008**, *130*, 12762–12774.
(9) Ando, T.; Kamigaito, M.; Sawamoto, M. *Macromolecules* **2000**, *33*, 2819–2824.
(10) Shipp, D. A.; Wang, J.-L.; Matyjaszewski, K. *Macromolecules* **1998**, *31*, 8005–8008.
(11) Coessens, V.; Pintauer, T.; Matyjaszewski, K. *Prog. Polym. Sci.* **2001**, *26*, 337–377.
(12) Matyjaszewski, K.; Xia, J. *Chem. Rev.* **2001**, *101*, 2921–2990.
(13) Tsarevsky, N. V.; Matyjaszewski, K. *Chem. Rev.* **2007**, *107*, 2270–2299.
(14) Oh, J. K.; Drumright, R.; Siegwart, D. J.; Matyjaszewski, K. *Prog. Polym. Sci.* **2008**, *33*, 448–477.
(15) Sheiko, S. S.; Sumerlin, B. S.; Matyjaszewski, K. *Prog. Polym. Sci.* **2008**, *33*, 759–785.
(16) Gao, H.; Matyjaszewski, K. *Prog. Polym. Sci.* **2009**, *34*, 317–350.
(17) Matyjaszewski, K.; Shipp, D. A.; Wang, J. L.; Grimaud, T.; Patten, T. E. *Macromolecules* **1998**, *31*, 6836–6840.
(18) Matyjaszewski, K.; Shipp, D. A.; McMurtry, G. P.; Gaynor, S. G.; Pakula, T. *J. Polym. Sci., Part A: Polym. Chem.* **2000**, *38*, 2023–2031.
(19) Matyjaszewski, K.; Paik, H.; Shipp, D. A.; Isobe, Y.; Okamoto, Y. *Macromolecules* **2001**, *34*, 3127–3129.
(20) Tang, C.; Kowalewski, T.; Matyjaszewski, K. *Macromolecules* **2003**, *36*, 1465–1473.
(21) Huang, J.; Jia, S.; Siegwart, D. J.; Kowalewski, T.; Matyjaszewski, K. *Macromol. Chem. Phys.* **2006**, *207*, 801–811.
(22) Ramakrishnan, A.; Dhamodharan, R. *Macromolecules* **2003**, *36*, 1039–1046.
(23) Stoffelbach, F.; Poli, R. *Chem. Commun.* **2004**, 2666–2667.
(24) Poli, R.; Stoffelbach, F.; Maria, S.; Mata, J. *Chem.—Eur. J.* **2005**, *11*, 2537–2548.
(25) Seeliger, F.; Matyjaszewski, K. *Macromolecules* **2009**, *42*, 6050–6055.
(26) Goto, A.; Fukuda, T. *Macromol. Rapid Commun.* **1999**, *20*, 633–636.

(27) Chambard, G.; Klumperman, B.; German, A. L. *Macromolecules* **2000**, *33*, 4417–4421.
(28) Matyjaszewski, K.; Paik, H. J.; Zhou, P.; Diamanti, S. J. *Macromolecules* **2001**, *34*, 5125–5131.
(29) Tang, W.; Matyjaszewski, K. *Macromolecules* **2006**, *39*, 4953–4959.
(30) Tang, W.; Matyjaszewski, K. *Macromolecules* **2007**, *40*, 1858–1863.
(31) Tang, W.; Kwak, Y.; Braunecker, W.; Tsarevsky, N. V.; Coote, M. L.; Matyjaszewski, K. *J. Am. Chem. Soc.* **2008**, *130*, 10702–10713.
(32) Tang, W.; Nanda, A. K.; Matyjaszewski, K. *Macromol. Chem. Phys.* **2005**, *206*, 1171–1177.
(33) Bortolamei, N.; Isse, A. A.; Di Marco, V. B.; Gennaro, A.; Matyjaszewski, K. *Macromolecules* **2010**, *43*, 9257–9267.
(34) Song, L.; Trogler, W. C. *J. Am. Chem. Soc.* **1992**, *114*, 3355–3361.
(35) Pintauer, T.; Matyjaszewski, K. *Coord. Chem. Rev.* **2005**, *249*, 1155–1184.
(36) Baisch, U.; Poli, R. *Polyhedron* **2008**, *27*, 2175–2185.
(37) Wulkow, M. *Macromol. Theory Simul.* **1996**, *5*, 393–416.